Protein Structure and Folding:

Structural Basis for Recognition of CD20 by Therapeutic Antibody Rituximab

Jiamu Du, Hao Wang, Chen Zhong, Baozhen Peng, Meilan Zhang, Bohua Li, Sheng Huo, Yajun Guo and Jianping Ding

J. Biol. Chem. 2007, 282:15073-15080.
doi: 10.1074/jbc.M701654200 originally published online March 29, 2007

THE JOURNAL OF BIOLOGICAL CHEMISTRY VOL. 282, NO. 20, pp. 15073–15080, May 18, 2007

Structural Basis for Recognition of CD20 by Therapeutic Antibody Rituximab*[S]

Received for publication, February 26, 2007, and in revised form, March 19, 2007 Published, JBC Papers in Press, March 29, 2007, DOI 10.1074/jbc.M701654200

Jiamu Du[‡§], Hao Wang[¶], Chen Zhong[‡], Baozhen Peng[‡], Meilan Zhang[‡], Bohua Li[¶], Sheng Huo[¶], Yajun Guo[¶1], and Jianping Ding[‡2]

From the [‡]State Key Laboratory of Molecular Biology, Institute of Biochemistry and Cell Biology, Shanghai Institutes for Biological Sciences, Chinese Academy of Sciences, and [§]Graduate School of Chinese Academy of Sciences, 320 Yue-Yang Road, Shanghai 200031, China and the [¶]International Joint Cancer Institute, Second Military Medical University, 800 Xiang-Yin Road, Shanghai 200433, China

Rituximab is a widely used monoclonal antibody drug for treating certain lymphomas and autoimmune diseases. To understand the molecular mechanism of recognition of human CD20 by Rituximab, we determined the crystal structure of the Rituximab Fab in complex with a synthesized peptide comprising the CD20 epitope (residues 163–187) at 2.6-Å resolution. The combining site of the Fab consists of four complementarity determining regions that form a large, deep pocket to accommodate the epitope peptide. The bound peptide assumes a unique cyclic conformation that is constrained by a disulfide bond and a rigid proline residue (Pro^{172}). The ^{170}ANPS^{173} motif of CD20 is deeply embedded into the pocket on the antibody surface and plays an essential role in the recognition and binding of Rituximab. The antigen-antibody interactions involve both hydrogen bonds and van der Waals contacts and display a high degree of structural and chemical complementarity. These results provide a molecular basis for the specific recognition of CD20 by Rituximab as well as valuable information for development of improved antibody drugs with better specificity and higher affinity.

CD20 is a pan-B cell marker expressed from pre-B cells until B cells are differentiated into plasma cells (1). It is a tetraspan membrane protein that is predicted to contain a large extracellular loop (about residues 142 to 182) and to form oligomers on the cell surface (2–4). Although the precise function of CD20 remains unclear, biochemical and cell biological data have shown that it seems to form or regulate a voltage-independent calcium channel (3, 5). Despite the limited knowledge about its function, several lines of evidence have clearly demonstrated that CD20 is an ideal target for passive immunotherapy of B-cell lymphoma: it is highly expressed in more than 80% of the B-cell lymphomas but not in stem cells, pro-B cells, normal plasma cells, or other normal tissues; it remains on the cell surface without substantial internalization after cross-linking with antibodies; and it is not shed to the circulation to inhibit the antibody therapy (6–8).

The CD20-targeted chimeric monoclonal antibody (mAb)[3] Rituximab (Rituxan,® IDEC-C2B8) was the first Food and Drug Administration approved mAb drug for the treatment of malignancy. Although it was originally used for treating low-grade non-Hodgkin lymphoma, Rituximab has been proven to be also effective against other types of lymphomas (9, 10) and some autoimmune diseases (11–13). Multiple mechanisms have been proposed for the action of Rituximab in the depletion of B cells including its ability to mediate complement-dependent cytotoxicity and antibody-dependent cellular cytotoxicity, and to induce cell apoptosis (reviewed in Refs. 14 and 15). With the expansion of the clinical application of Rituximab in the treatment of lymphoproliferative diseases, it has been noticed that intensity of CD20 expression on B cells varies in patients that may affect the binding and efficacy of Rituximab therapy (16, 17). Therefore, it is rational to expect that new antibodies with higher affinity and better specificity developed based on Rituximab might be beneficial in clinical use, especially for patients who have low expression levels of CD20.

Besides Rituximab and Zevalin® (the prototype of Rituximab 2B8 attached by a radioactive substance ^{90}Y), another mAb specific to human CD20, namely B1, in both native and radioderivative forms (Bexxar,® Tositumomab and ^{131}I-Tositumomab), was approved by the Food and Drug Administration for the treatment of non-Hodgkin lymphoma in 2003 (18). These antibody drugs along with some other mAbs against CD20 such as 1F5, AT80, and 2H7 were suggested to most likely recognize the same region (Tyr^{165} to Tyr^{182}) of the large extracellular loop of human CD20 with fine specificities (2, 19). However, these antibodies vary considerably in their functional activities. For example, treatment of B cells with most mAbs promotes segregation of CD20 into detergent-insolu-

* This work was supported by Ministry of Science and Technology of China Grants 2004CB720102, 2004CB720101, 2006CB806501, and 2006AA02Z112 and National Natural Science Foundation of China Grant 30570379. The costs of publication of this article were defrayed in part by the payment of page charges. This article must therefore be hereby marked "*advertisement*" in accordance with 18 U.S.C. Section 1734 solely to indicate this fact.

[S] The on-line version of this article (available at http://www.jbc.org) contains supplemental Fig. S1.

The atomic coordinates and structure factors (code 2OSL) have been deposited in the Protein Data Bank, Research Collaboratory for Structural Bioinformatics, Rutgers University, New Brunswick, NJ (http://www.rcsb.org/).

[1] To whom correspondence may be addressed: 800 Xiang-Yin Rd., Shanghai 200433, China. Tel.: 086-21-2507-0241; Fax: 086-21-2507-4349; E-mail: yjguo@smmu.edu.cn.

[2] To whom correspondence may be addressed: 320 Yue-Yang Rd., Shanghai 200031, China. Tel.: 086-21-5492-1619; Fax: 086-21-5492-1116; E-mail: jpding@sibs.ac.cn.

[3] The abbreviations used are: mAb, monoclonal antibody; CDRs, complementarity determining regions; H, heavy chain; L, light chain.

ble lipid raft, whereas B1 is the exception. This property seems to be correlated with the ability of the antibodies to mediate complement-dependent cytotoxicity but irrespective of activation of cell apoptosis pathways (20–22).

To understand the functional diversity of CD20 mAbs and the underlying mechanisms, identification of the epitope of CD20 recognized by Rituximab and other CD20-targeted mAbs has raised great interest in recent years. Sequence comparison of human and murine CD20 reveals that although the two species share 73% sequence identity, the large extracellular loop is less conserved as 16 of the approximate 43 amino acids are different (19). Mutagenesis studies by exchanging variant residues of the large extracellular loop between human CD20 and mouse CD20 at the equivalent position indicate that residues Ala^{170} and Pro^{172} of human CD20 are critical determinants for the CD20 epitope (19). Using a process of biopanning of a phage display peptide library consisting of randomized 7-mer cyclic peptides, it has been shown that an NPS motif corresponding to ^{171}NPS^{173} of human CD20 is essential for Rituximab binding and Ala^{170} can be substituted by Ser (4). Similar studies have also defined a discontinuous epitope that comprises ^{170}ANPS^{173} and ^{182}YCYSI^{185} of CD20 joined together spatially by a disulfide bond between Cys^{167} and Cys^{183} (23). However, the underlying mechanism of the recognition and binding of Rituximab with the CD20 epitope remains unclear.

We report here the crystal structure of the Rituximab Fab fragment in complex with an epitope peptide of the large extracellular loop (residues 163–187) of CD20 that provides the molecular basis for the antigen-antibody recognition and binding. Analysis of the complex structure explains very well biochemical data from the epitope-mapping studies and provides useful hints for the design and development of improved antibody drugs.

EXPERIMENTAL PROCEDURES

Preparation of Antibody and Peptide—Rituximab was purchased from Roche. The Fab fragment was obtained by papain digestion of Rituximab and purified by cation exchange chromatography using SP-Sepharose FF (GE Healthcare) followed by hydrophobic interaction chromatography using phenyl-Sepharose HP (GE Healthcare). The purity and homogeneity of the Fab fragment was characterized by SDS-PAGE and dynamic light scattering analyses. The protein sample was concentrated to 8 mg/ml and then exchanged into a stock buffer (100 mM NaCl and 10 mM Tris-HCl, pH 8.0) for crystallization. The amino acid sequence of the Fab fragment was determined according to United States patent 5843439 (42).

A 25-mer cyclic peptide (NIYNCEPANPSEKNSPSTQYCYSIQ) corresponding to residues 163–187 of the large extracellular loop of human CD20 was synthesized in which an intrachain disulfide bond was introduced between Cys^{167} and Cys^{183} (Shanghai Science Peptide Biological Technology). The quality of the peptide was determined by analytical reverse-phase chromatography and mass spectral analysis with a purity of greater than 95%.

Crystallization and Diffraction Data Collection—Initial crystallization trials of the Rituximab Fab fragment itself yielded large crystals that, however, did not diffract x-ray beyond 7-Å resolution and could not be used for structure determination. For co-crystallization experiments, the purified Rituximab Fab and the epitope peptide were mixed at a molar ratio of 1:5 at 4 °C for 12 h. Co-crystallization was carried out using the hanging drop vapor diffusion method by mixing equal volumes of the protein/peptide mixture solution and a reservoir solution (0.2 M calcium acetate, 0.1 M sodium cacodylate, pH 6.5, and 18% PEG8000). Square shaped crystals grew to a maximum size of $0.1 \times 0.1 \times 0.2$ mm^3 at 4 °C in 2 weeks. For diffraction data collection, crystals were cryostabilized by Paratone-N (Hampton Research) and then flash-cooled to −170 °C. Diffraction data were collected to 2.6-Å resolution at beamline NW12 of Photon Factory, Japan, and processed using suite HKL2000 (24). Statistics for diffraction data are summarized in Table 1.

Structure Determination, Refinement, and Analysis—The structure of the Rituximab Fab in complex with human CD20 epitope peptide was solved using the molecular replacement method as implemented in Phaser (25). The structure of the Fab fragment of human mAb A5B7 (26) (Protein Data Bank code 1AD0) was used as the search model. Structure refinement was carried out by CNS using standard protocols consisting of conjugate-gradient energy minimization, torsion-constrained molecular dynamics simulated annealing, group B factor refinement, and individual *B* factor refinement (27). Free *R* factor was calculated using 5% randomly selected reflections. After several cycles of manual model building using program O (28), the electron density was further improved and clear enough for tracing the epitope peptide without ambiguity. The stereochemistry of the structure model was analyzed with Procheck (29). Statistics of the structure refinement are also summarized in Table 1. Structural analysis was mainly performed using CNS (27) and programs in the CCP4 suite (29). The elbow angle of the Fab fragment was calculated with the method described by Stanfield *et al.* (30). Figures were prepared using programs Ribbons (31) and Pymol (32).

RESULTS AND DISCUSSION

Overall Structure of the Rituximab Fab-CD20 Epitope Peptide Complex—Recent studies have identified the epitope of CD20 recognized by Rituximab being a sequence motif located at the large extracellular loop of CD20 consisting of ^{170}ANPS^{173} (4, 19, 23). To understand the structural basis of the recognition of CD20 by Rituximab, we synthesized a 25-mer peptide mimic of the epitope of CD20 comprising the CD20 sequence from Asn^{163} to Gln^{187} (numbered according to the CD20 sequence). To mimic the conformation of the CD20 epitope, an intrachain disulfide bond was introduced between residues Cys^{167} and Cys^{183} of the synthesized peptide because such linkage has been found in human CD20 expressed in *Escherichia coli* and probably exists naturally (33). This disulfide linkage has also been implicated to play an important role in the recognition and binding of the epitope by Rituximab because disruption of the disulfide bond abolishes the binding of CD20 to Rituximab and reconstruction of the disulfide bond can partially restore the binding (33). The peptide was conjugated to a protein carrier keyhole limpet hemocyanin and shown to have similar reactivity with Rituximab as the keyhole limpet hemocyanin-

TABLE 1
Summary of diffraction data and structure refinement statistics

Summary of diffraction data	
Wavelength (Å)	1.0000
Space group	$P2_12_12_1$
Cell parameters	
a (Å)	96.4
b (Å)	98.8
c (Å)	107.2
Resolution range (Å)	50.0–2.60 (2.69–2.60)[a]
Observed reflections	119,890
Unique reflections ($I/\sigma(I) > 0$)	29,570
Average redundancy	4.1 (3.7)
Average $I/\sigma(I)$	17.8 (2.0)
Completeness (%)	90.6 (91.5)
R_{merge} (%)[b]	7.6 (43.4)
Statistics of refinement and model	
Number of reflections ($F_o > 0\sigma(F_o)$)	
Working set	29,131
Free *R* set	1,460
R factor (%)[c]	23.9 (35.6)
Free *R* factor (%)	29.6 (42.8)
Number of residues	913
Number of water molecules	212
Average B factor of all atoms (Å^2)	49.0
Complex/Fab fragment/peptide	49.2/49.0/54.6
Water molecule	40.3
Root mean square bond lengths (Å)	0.008
Root mean square bond angles (°)	1.6
Luzzati atomic position error (Å)	0.37
Ramachandran plot (%)	
Most favored regions	87.4
Allowed regions	11.6
Generously allowed regions	0.8
Disallowed regions	0.3

[a] Numbers in parentheses refer to the highest resolution shell.
[b] $R_{merge} = \Sigma_{hkl}\Sigma_i|I_i(hkl)_i - \langle I(hkl)\rangle|/\Sigma_{hkl}\Sigma_i I_i(hkl)$.
[c] *R* factor $= ||F_o| - |F_c||/|F_o|$.

conjugated cyclic peptides Rp15-C and Rp3-C (4) by the enzyme-linked immunosorbent assay binding assay (supplementary Fig. S1*A*). Specificity of the reactivity was also confirmed by peptide blocking assays with immunofluorescence and complement-dependent cytotoxicity using Raji cells (supplementary Fig. S1, *B* and *C*).

The CD20 epitope peptide was co-crystallized in complex with the Rituximab Fab fragment. The structure of the complex was solved using molecular replacement and refined to a resolution of 2.6 Å with an *R* factor of 23.9% and a free *R* factor of 29.6% (Table 1). There are two Fab-peptide complexes (A and B) in the crystallographic asymmetric unit. The two complexes adopt very similar conformation (root mean square deviation of 0.96 Å for 449 Cα atoms) except that the heavy chain in complex A contains three more residues at the C terminus than in complex B and two extra residues can be visualized at the N terminus of the peptide chain in complex B than in complex A. Due to the better electron density quality, the structure model of complex A will be used for further structural analysis and discussion. Chain identifiers L, H, and P are designated to identify the light chain and heavy chain of the Fab fragment and the epitope peptide, respectively (Fig. 1).

Overall the Rituximab Fab has very good electron density, except residues from Ser^{H135} to Gly^{H141} of a loop in the constant region that have high *B* factors above 80 Å^2 compared with the average *B* factor of 49 Å^2 for the whole model. The Rituximab Fab has a canonical immunoglobulin fold consisting of four β-barrel domains (Fig. 1*A*). The light chain comprises residues Leu^1 to Leu^{213} that fold into the V_L and C_L domains, and heavy chain residues His^1 to His^{224} that fold into the V_H and C_H domains. The elbow angle made by the two pseudo 2-fold axes that define the relative disposition of V_H to V_L and C_H to C_L is about 139°. There are four intra-domain disulfide bonds between Cys^{L23} and Cys^{L87}, Cys^{L133} and Cys^{L193}, Cys^{H22} and Cys^{H96}, and Cys^{H148} and Cys^{H204}, and one inter-domain disulfide bond between Cys^{L213} and Cys^{H224}. Like other Fab structures, residue Thr^{50} of the light chain (Thr^{L50}) lies in the disallowed region of the Ramachandran plot and forms part of the classic γ-turn (34). The complementarity determining regions (CDRs) of the Rituximab Fab have ordinary length without unusual residues according to Kabat sequence data base searching (35). The CDR loops L1, L2, L3, H1, and H2 belong to Chothia canonical classes (34) 1, 1, 1, 1, and 2, respectively. The CDR loops L3, H1, H2, and H3 together form a large, deep pocket to accommodate the epitope peptide, whereas loops L1 and L2 are located behind loops L3 and H3 (Fig. 1*A*).

The electron density for the bound epitope peptide is well defined without ambiguity in the positioning of the main chains and side chains (Fig. 1*B*). Residues Cys^{P167} and Cys^{P183} of the peptide form a disulfide bond that drags the termini of the peptide together covalently and makes the peptide to adopt a unique cyclic conformation (Fig. 1*C*). The N-terminal part of the peptide (Cys^{P167} to Asn^{P171}) forms a short coil that is stabilized by the tense restraints of the disulfide bond and the hydrogen-bonding interactions between residues of the coil and the CDRs of the Rituximab Fab. The middle part of the peptide forms a short 3_{10} helix (Pro^{P172} to Glu^{P174}) and a small loop (Lys^{P175} to Ser^{P177}) that are stabilized by hydrogen-bonding interactions with the other regions (Table 2 and Fig. 1*C*). The C-terminal part of the peptide (Pro^{P178} to Tyr^{P184}) forms a short α-helix of hydrophobic nature (Tyr^{P182}, Tyr^{P184}, and Ile^{P186}). Considering it is at the end of the extracellular loop and must be close to the cell membrane, this short α-helix might be the extension of a long transmembrane α-helix of CD20 as predicted by PredictProtein Server (36).

Interactions between the Rituximab Fab and the Epitope Peptide—Rituximab can bind to CD20 on B cells with a binding affinity of 5 nM (37). In the complex structure, the epitope peptide of human CD20 is bound at the large pocket formed by CDR loops L3, H1, H2, and H3 of the Rituximab Fab (Fig. 2*A*), which is consistent with the observation that the heavy chain CDRs usually make more contributions than the light chain CDRs in antigen binding especially when Fab binds with a small antigen (38, 39). The binding of the epitope peptide with the Fab buries a solvent accessible surface area of about 440 Å^2 (calculated with a probe radius of 1.4 Å) which is about 23% of the peptide surface (1911 Å^2) or 2.3% of the Fab surface (19403 Å^2). Although the buried surface area is within the average range of the protein-peptide complexes (400–700 Å^2) (40), the peptide fits the CDR regions of the Rituximab Fab quite well with a high degree of structural and chemical complementarity (Fig. 2*B*) as indicated by the high shape complementarity value (Sc) of 0.83 (calculated with default parameters) compared with the average Sc value of 0.64–0.68 for antibody-antigen complexes (41).

The CDR loops L3, H1, H2, and H3 of the Fab participate in interactions primarily with four residues, ^{170}ANPS^{173}, of the epitope peptide that have been shown to be a critical motif on

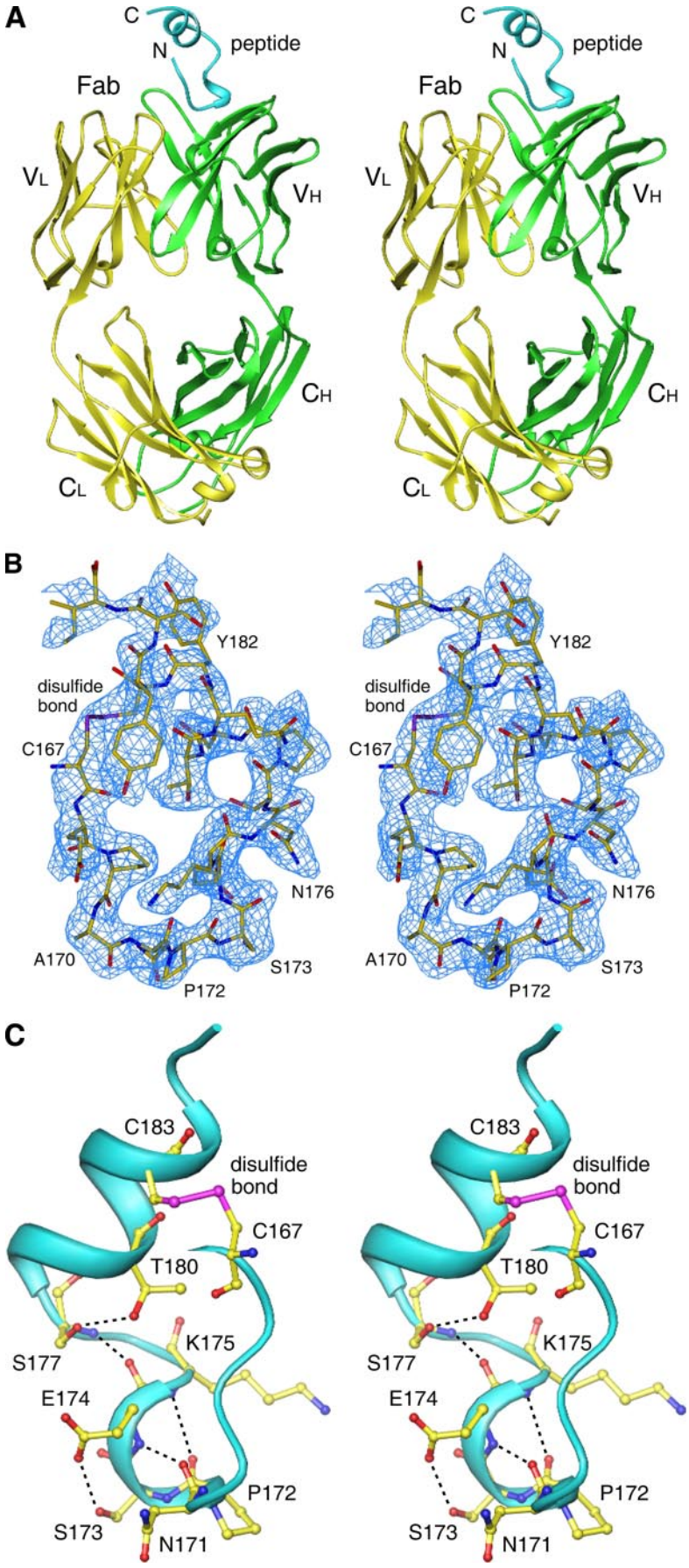

TABLE 2
Hydrogen-bonding interactions between the middle part of the peptide and the other regions of the peptide

Donor	Acceptor	Distance
		Å
Glu^{P174}-N	Asn^{P171}-O	3.08
Ser^{P173}-O^{γ}	Glu^{P174}-$O^{\epsilon 2}$	2.93
Lys^{P175}-N	Pro^{P172}-O	3.15
Ser^{P177}-N	Glu^{P174}-O	2.69
Ser^{P177}-O^{γ}	Thr^{P180}-$O^{\gamma 1}$	2.76

the CD20 surface for antibody recognition (2, 4, 23). Residues of the motif form a network of hydrogen bonds with residues of the surrounding CDR loops (Table 3 and Fig. 2, *C* and *D*). Specifically, the side chain of Asn^{P171} forms two hydrogen bonds with the side chains of Ser^{H99} and Trp^{H106} of the H3 loop, respectively. The main chain carbonyl of Pro^{P172} forms a hydrogen bond with the side chain of Asn^{H55} of loop H2 via a water molecule; and the main chain amide and side chain O^{γ} of Ser^{P173} make two hydrogen bonds with the side chain of Asn^{H33} of loop H1, respectively. Moreover, the residues flanking the motif including Glu^{P168}, Pro^{P169}, and Lys^{P175} also contribute to the interactions of the peptide with the Fab by forming hydrogen bonds with Asn^{L93}, Ser^{H59}, and Thr^{H58}, respectively (Table 3 and Fig. 2, *C* and *D*). In addition to these hydrogen-bonding interactions, extensive van der Waals contacts are observed between residues 168 and 179 of the peptide and the Fab (Table 4). In particular, the ^{170}ANPS^{173} motif contributes 79 of the 97 van der Waals contacts between the peptide and the Fab (Table 4). These interactions can partially explain the high affinity of Rituximab with human CD20.

In addition, Pro^{P172} of the ^{170}ANPS^{173} motif that has been shown to play an essential role in the antigen-antibody recognition (4, 19), is located at the bottom of the CDR pocket (Fig. 2*B*) formed by residues Ala^{H50}, Tyr^{H52}, Asp^{H57}, and Ser^{H59} of loop H2 of the Fab and residue Asn^{H33} of loop H1, and has both hydrophilic and hydrophobic interactions with the surrounding residues of the Fab. The special position of Pro^{P172} at the turn of the 3_{10} helix and the rigid conformation of proline might play an important role in maintaining the unique conformation of the peptide and hence in the recognition and binding of Rituximab.

Structural Basis for the Specificity of Rituximab—Human CD20 is an important drug target for the treatment of lymphomas. Rituximab is the first Food and Drug Administration approved mAb drug against CD20 for the treatment of B cell non-Hodgkin lymphoma, and now has been used to treat autoimmune diseases and reduce the alloreaction in organic transplantations. Our crystal structure of the Rituximab Fab in complex with a 25-mer peptide mimicking the epitope on the large extracellular loop of human CD20 has provided a molecular basis for understanding the underlying mechanisms of the recognition and binding of CD20 with its antibodies and will be valuable in the modification of Rituximab for development of more effective mAb drugs against non-Hodgkin lymphoma and other diseases.

Screenings of phage display peptide libraries that can express 7-mer cyclic and 7-/12-mer linear peptides have shown that the sequence motif A(S)NPS corresponding to ^{170}ANPS^{173} of the large extracellular loop of human CD20 is the most important region for Rituximab recognition and binding (4, 23). In particular, Ala^{170} and Pro^{172} are the most critical ones determined by means of phage display, mutagenesis, and peptide scanning (2, 4, 19). In our structure of the Rituximab Fab-CD20 epitope-peptide complex, four residues ^{170}ANPS^{173} of the motif are deeply buried in the pocket formed by four CDR loops (L3, H1, H2, and H3). Ala^{170} is located in a hydrophobic cavity formed by Trp^{L47}, Trp^{L90}, Asn^{L93}, and Pro^{L95} of the Fab. The space of the cavity is too narrow to accommodate other residues with a large side chain except serine due to steric conflict (Fig. 2*B*), providing an explanation for the result that only serine is interchangeable with Ala^{170} (4). Similarly, Pro^{172} is positioned at the tip of the 3_{10} helix and is bound at the bottom of the CDR pocket (Fig. 2*B*). Modeling study indicates that a serine residue could fit at the same site. However, the relaxation of the rigid conformation of Pro^{172} might disrupt the conformational constraint of the 3_{10} helix and hence reduce the specificity and binding affinity, which explains the result that when Pro^{172} was substituted by serine in the cyclic 7-mer peptide, the mutant peptide could not bind to Rituximab (4).

The importance and requirement of the two other residues, Asn^{171} and Ser^{173}, of the motif are also supported by our crystal structure showing that each residue makes two of total eight hydrogen bonds as well as extensive van der Waals contacts with the Rituximab Fab. In the structure model, six residues (Glu^{168}, Pro^{169}, Asn^{171}, Pro^{172}, Ser^{173}, and Lys^{175}) of the epitope peptide make hydrogen-bonding interactions, and additionally Ala^{170}, Glu^{174}, Asn^{176}, and Ser^{179} make van der Waals contacts with the Rituximab Fab. Although only ^{170}ANPS^{173} of CD20 were documented to be involved in the Rituximab binding, the other residues might also play some roles in the recognition and binding of CD20 by Rituximab.

Based on phage display results, it was suggested that fragment ^{182}YCYSI^{186} at the C terminus of the large extracellular loop of CD20 is also involved in Rituximab binding (23). In our structure, this region forms part of the C-terminal α-helix and has no direct interaction with the Fab. However, residues Cys^{P183} and Cys^{P167} of the epitope peptide form a disulfide bond that makes the peptide adopt a unique cyclic conformation. In search for the epitope of CD20 with phage display peptide libraries, a series of cyclic and linear peptides were obtained; however, only the cyclic peptides match the sequence of human CD20 (4). Biochemical data have shown that disruption of the disulfide bond on the large extracellular loop of

FIGURE 1. **Overall structure of the Rituximab Fab-CD20 epitope-peptide complex.** *A*, overall structure of the complex. The Rituximab Fab is colored with the light chain in *yellow* and the heavy chain in *green*, and the CD20 epitope peptide in *cyan*. *B*, a stereoview of a composite-omit electron density map at 2.6-Å resolution for the bound epitope peptide contoured at 1.0-σ level. The atomic coordinates of the peptide residues are shown in ball and stick models. *C*, structure of the bound epitope peptide. The epitope peptide consists of a short N-terminal coil (residues 167–171), a 3_{10} helix (residues 172–174), a small loop (residues 175–177), and a short C-terminal α-helix (residues 178–184). The intra-peptide hydrogen-bonding interactions between residues of the middle part (the 3_{10} helix and the small loop) and the other parts of the peptide are indicated with *dashed lines*.

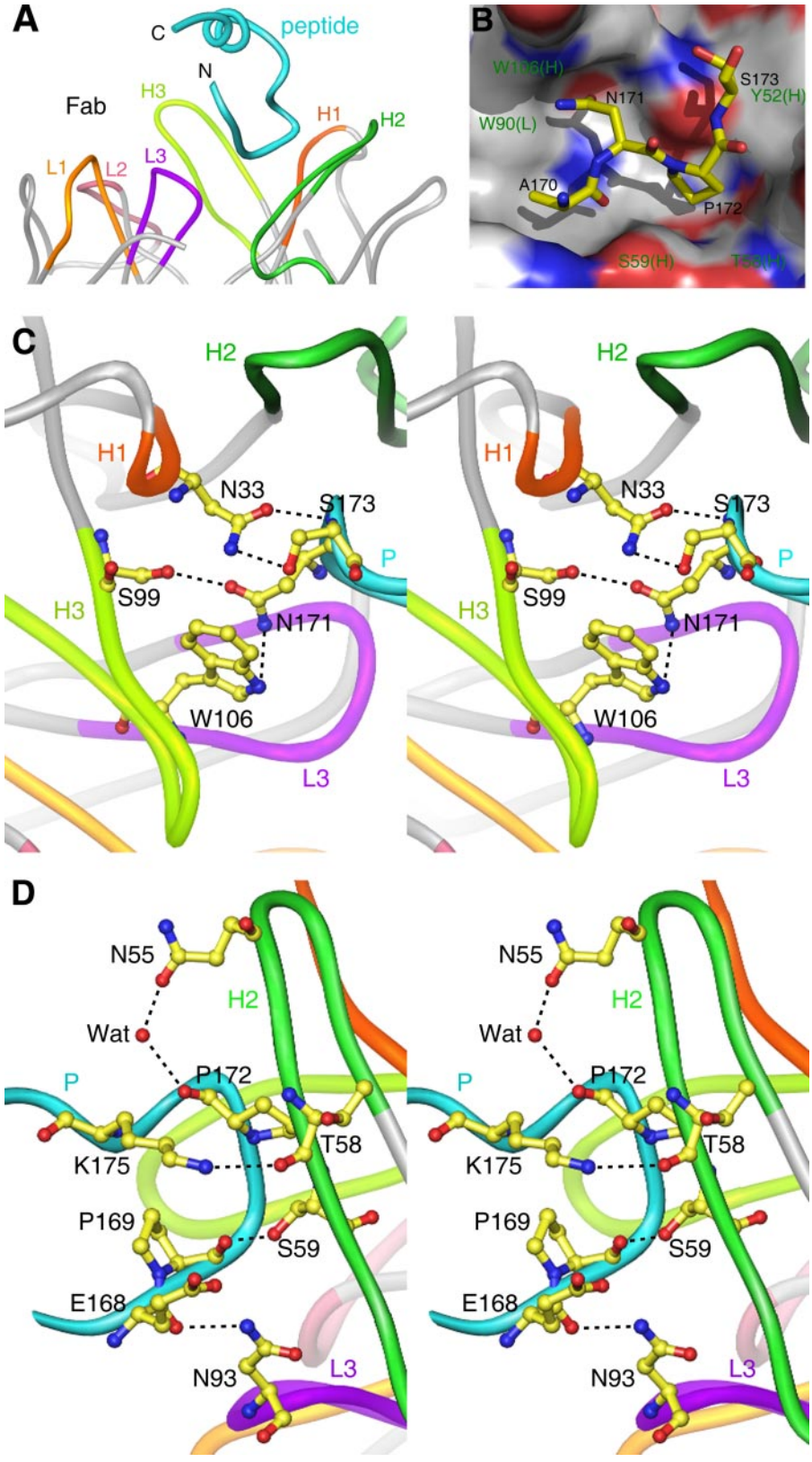

FIGURE 2. **Interactions between the Rituximab Fab and the epitope peptide.** *A*, an overview showing the interactions of the epitope peptide with the Rituximab Fab. The Fab CDRs are shown with the H1 loop in *orange*, H2 in *green*, H3 in tinted *green*, L1 in *gold*, L2 in *pink*, and L3 in *purple*. The peptide is colored in *cyan*. The four CDR loops (H1, H2, H3, and L3) of the Fab form a pocket to accommodate the epitope peptide. *B*, an electrostatic potential surface of the Rituximab Fab in the region of the epitope peptide binding pocket showing the structural and chemical complementarity between the Fab and the bound peptide. The residues of the epitope peptide involved in interactions with the Fab are shown with ball and stick models. The ^{170}ANPS^{173} motif of the CD20 epitope is located in a pocket formed by CDR loops H1, H2, H3, and L3 of the Fab. The locations of a few residues of the Fab are labeled for reference. *C*, a stereoview showing the hydrogen-bonding interactions between residues of the epitope peptide and CDR loops H1 and H3 of the Fab. The color coding of the structural elements is the same as *A*. *D*, a stereoview showing the hydrogen bonding between the epitope peptide and CDR loops H2 and L3 of the Fab.

TABLE 3
Hydrogen-bonding interactions between the Rituximab Fab CDRs and the epitope peptide

Peptide atom	Fab atom	CDR loop	Distance
			Å
Glu^{P168}-O	Asn^{L93}-$N^{\delta2}$	L3	2.94
Pro^{P169}-O	Ser^{H59}-O^{γ}	H2	2.75
Asn^{P171}-$O^{\delta1}$	Ser^{H99}-O^{γ}	H3	2.79
Asn^{P171}-$N^{\delta2}$	Trp^{H106}-N^{ξ}	H3	3.10
Pro^{P172}-O	Asn^{H55}-$O^{\delta1}$	H2	2.66/2.97[a]
Ser^{P173}-N	Asn^{H33}-$O^{\delta1}$	H1	2.93
Ser^{P173}-O^{γ}	Asn^{H33}- $N^{\delta2}$	H1	3.06
Lys^{P175}-N^{ξ}	Thr^{H58}-O	H2	3.12

[a] Hydrogen bond mediated by water molecule. The number before the slash is the distance between the Fab atom and the water molecule, and the number after the slash is the distance between the water molecule and the peptide atom.

TABLE 4
van der Waals contacts between the Rituximab Fab CDRs and the epitope peptide (≤4.0 Å)

Peptide residues	Rituximab Fab residues
Glu^{P168}	Asn^{L93} (4),[a] Ser^{H59} (1)
Pro^{P169}	Asn^{L93} (2), Ser^{H59} (2)
Ala^{P170}	Trp^{L90} (1), Asn^{L93} (4), Pro^{L95} (1), His^{H35} (1), Trp^{H47} (2), Ala^{H50} (1), Ser^{H59} (3)
Asn^{P171}	Trp^{L90} (6), Asn^{H33} (8), His^{H35} (2), Ser^{H99} (2), Trp^{H106} (18)
Pro^{P172}	Asn^{H33} (4), Ala^{H50} (4), Ile^{H51} (2), Tyr^{H52} (1), Asp^{H57} (3), Thr^{H58} (1), Ser^{H59} (2)
Ser^{P173}	Asn^{H33} (7), Tyr^{H52} (6)
Glu^{P174}	Tyr^{H102} (6), Trp^{H106} (2)
Lys^{P175}	Asp^{H57} (1)

[a] Numbers in parentheses refer to the number of van der Waals contacts.

CD20 completely ablates the binding of CD20 with Rituximab (33). It is very likely that the involvement of the C-terminal ^{182}YCYSI^{186} fragment of the large extracellular loop in the recognition and binding of Rituximab is through the formation of the disulfide bond and the constraint and stabilization of the cyclic conformation of the epitope rather than direct interaction with the antibody.

Analysis of the crystal structure of the Rituximab Fab in complex with its epitope peptide also provides valuable information for modification of the antibody to improve the specificity and binding affinity. Changes of residues on the CDR loops of the Rituximab Fab that could generate more favorable interactions with residues of the epitope of CD20 might increase its binding affinity and specificity with CD20. For instance, substitution of Ser^{H59} with a polar residue having a slightly longer side chain could introduce favorable hydrophilic interactions with the side chains of Glu^{P168} and/or Lys^{P175}. Change of Asp^{H57} to Glu could generate more hydrophilic interactions with the side chain of Lys^{P175} and/or Asn^{P176}. Mutation of Asn^{H55} to Gln might form potential hydrogen bonds with the side chain of Asn^{P176}. Similarly, substitution of Tyr^{H102} with a basic residue such as Lys might form a salt bridge with the side chain of Glu^{P174} and/or hydrophilic interaction with the side chain of Ser^{P179}. Substitution of Trp^{H106} with a basic residue like Lys might form new hydrophilic interactions with the side chain of Asn^{P171} and Glu^{P174}.

In summary, we report here the crystal structure of the Fab fragment of therapeutic antibody Rituximab in complex with its epitope peptide of human CD20. Structural analysis reveals the molecular basis of the specific recognition and binding of CD20 by Rituximab. Specifically, the most important epitope region ^{170}ANPS^{173} on the large extracellular loop of CD20 is bound at a pocket formed by four CDR loops of the Rituximab Fab and recognized by residues of the CDR loops through a network of hydrogen-bonding interactions and extensive van der Waals contacts. The unique cyclic conformation of the epitope peptide, which is attributed to the formation of a disulfide bond between Cys^{P167} and Cys^{P183} and the presence of a rigid Pro^{P172}, forms the basis of the specificity of Rituximab. Our structural results also provide useful hints for the development of new therapeutic antibodies with higher binding affinity and better specificity for the treatment of non-Hodgkin lymphoma.

Acknowledgments—We are grateful to the staff members at Photon Factory, Japan, for support in diffraction data collection, and other members of our laboratories for technical assistance and helpful discussions.

REFERENCES

1. Stashenko, P., Nadler, L. M., Hardy, R., and Schlossman, S. F. (1980) *J. Immunol.* **125,** 1678–1685
2. Teeling, J. L., Mackus, W. J., Wiegman, L. J., van den Brakel, J. H., Beers, S. A., French, R. R., van Meerten, T., Ebeling, S., Vink, T., Slootstra, J. W., Parren, P. W., Glennie, M. J., and van de Winkel, J. G. (2006) *J. Immunol.* **177,** 362–371
3. Bubien, J. K., Zhou, L. J., Bell, P. D., Frizzell, R. A., and Tedder, T. F. (1993) *J. Cell Biol.* **121,** 1121–1132
4. Perosa, F., Favoino, E., Caragnano, M. A., and Dammacco, F. (2006) *Blood* **107,** 1070–1077
5. Li, H., Ayer, L. M., Lytton, J., and Deans, J. P. (2003) *J. Biol. Chem.* **278,** 42427–42434
6. Anderson, K. C., Bates, M. P., Slaughenhoupt, B. L., Pinkus, G. S., Schlossman, S. F., and Nadler, L. M. (1984) *Blood* **63,** 1424–1433
7. Press, O. W., Howell-Clark, J., Anderson, S., and Bernstein, I. (1994) *Blood* **83,** 1390–1397
8. Cragg, M. S., Walshe, C. A., Ivanov, A. O., and Glennie, M. J. (2005) *Curr. Dir. Autoimmun.* **8,** 140–174
9. Leget, G. A., and Czuczman, M. S. (1998) *Curr. Opin. Oncol.* **10,** 548–551
10. Boye, J., Elter, T., and Engert, A. (2003) *Ann. Oncol.* **14,** 520–535
11. Check, E. (2004) *Nature* **428,** 786
12. Edwards, J. C., Szczepanski, L., Szechinski, J., Filipowicz-Sosnowska, A., Emery, P., Close, D. R., Stevens, R. M., and Shaw, T. (2004) *N. Engl. J. Med.* **350,** 2572–2581
13. Cohen, Y., and Nagler, A. (2004) *Autoimmun. Rev.* **3,** 21–29
14. Smith, M. R. (2003) *Oncogene* **22,** 7359–7368
15. Jazirehi, A. R., and Bonavida, B. (2005) *Oncogene* **24,** 2121–2143
16. Keating, M., and O'Brien, S. (2000) *Semin. Oncol.* **27,** 86–90
17. McLaughlin, P., Hagemeister, F. B., Rodriguez, M. A., Sarris, A. H., Pate, O., Younes, A., Lee, M. S., Dang, N. H., Romaguera, J. E., Preti, A. H., McAda, N., and Cabanillas, F. (2000) *Semin. Oncol.* **27,** 37–41
18. Garber, K. (2003) *J. Natl. Cancer Inst.* **95,** 189
19. Polyak, M. J., and Deans, J. P. (2002) *Blood* **99,** 3256–3262
20. Deans, J. P., Robbins, S. M., Polyak, M. J., and Savage, J. A. (1998) *J. Biol. Chem.* **273,** 344–348
21. Cragg, M. S., Morgan, S. M., Chan, H. T., Morgan, B. P., Filatov, A. V., Johnson, P. W., French, R. R., and Glennie, M. J. (2003) *Blood* **101,** 1045–1052
22. Chan, H. T., Hughes, D., French, R. R., Tutt, A. L., Walshe, C. A., Teeling, J. L., Glennie, M. J., and Cragg, M. S. (2003) *Cancer Res.* **63,** 5480–5489
23. Binder, M., Otto, F., Mertelsmann, R., Veelken, H., and Trepel, M. (2006) *Blood* **108,** 1975–1978
24. Otwinowski, Z., and Minor, W. (1997) *Methods Enzymol.* **276,** 307–326
25. McCoy, A. J., Grosse-Kunstleve, R. W., Storoni, L. C., and Read, R. J. (2005)

Acta Crystallogr. Sect. D Biol. Crystallogr. **61,** 458–464
26. Banfield, M. J., King, D. J., Mountain, A., and Brady, R. L. (1997) *Proteins* **29,** 161–171
27. Brunger, A. T., Adams, P. D., Clore, G. M., DeLano, W. L., Gros, P., Grosse-Kunstleve, R. W., Jiang, J. S., Kuszewski, J., Nilges, M., Pannu, N. S., Read, R. J., Rice, L. M., Simonson, T., and Warren, G. L. (1998) *Acta Crystallogr. Sect. D Biol. Crystallogr.* **54,** 905–921
28. Jones, T. A., Zou, J. Y., Cowan, S. W., and Kjeldgaard, M. (1991) *Acta Crystallogr. Sect. A* **47,** 110–119
29. Collaborative Computational Project Number 4 (1994) *Acta Crystallogr. Sect. D Biol. Crystallogr.* **50,** 760–763
30. Stanfield, R. L., Zemla, A., Wilson, I. A., and Rupp, B. (2006) *J. Mol. Biol.* **357,** 1566–1574
31. Carson, M. (1997) *Methods Enzymol.* **277,** 493–502
32. DeLano, W. L. (2002) *Pymol*, pymol.sourceforge.net
33. Ernst, J. A., Li, H., Kim, H. S., Nakamura, G. R., Yansura, D. G., and Vandlen, R. L. (2005) *Biochemistry* **44,** 15150–15158
34. Al-Lazikani, B., Lesk, A. M., and Chothia, C. (1997) *J. Mol. Biol.* **273,** 927–948
35. Martin, A. C. (1996) *Proteins* **25,** 130–133
36. Rost, B., Yachdav, G., and Liu, J. (2004) *Nucleic Acids Res.* **32,** W321–W326
37. Reff, M. E., Carner, K., Chambers, K. S., Chinn, P. C., Leonard, J. E., Raab, R., Newman, R. A., Hanna, N., and Anderson, D. R. (1994) *Blood* **83,** 435–445
38. Davies, D. R., Padlan, E. A., and Sheriff, S. (1990) *Annu. Rev. Biochem.* **59,** 439–473
39. Wilson, I. A., and Stanfield, R. L. (1994) *Curr. Opin. Struct. Biol.* **4,** 857–867
40. Stanfield, R. L., and Wilson, I. A. (1995) *Curr. Opin. Struct. Biol.* **5,** 103–113
41. Lawrence, M. C., and Colman, P. M. (1993) *J. Mol. Biol.* **234,** 946–950
42. Anderson, D. R., Hanna, N., Leonard, J. E., Newman, R. A., Reff, M. E., and Rastetter, W. H. (December 1, 1998) U. S. patent 5843,439